

Depiction of the Ambipolar-State of the Gas-Substrate Interphase of
the Electron Cyclotron Resonance – Microwave – Chemical Vapor
Deposition (ECR-MW-CVD) Method and Its Influence over the
Properties of Vapor-Deposited Hydrocarbon Films

by

Jesús M Garcia-Figueroa

Submitted in Partial Fulfillment

of the

Requirements for the Degree

Doctor of Philosophy

Supervised by

Professor David R. Harding

Department of Chemical Engineering

Arts, Sciences, and Engineering

Edmund A. Hajim School of Engineering and Applied Sciences

University of Rochester

Rochester, New York

2022

Table of Contents

Biographical Sketch	xii
Abstract	xiv
Contributors and Funding Sources	xv
List of Tables	xvi
List of Figures	xxiv
List of Equations	xxxii
List of Symbols	xxxiii
Chapter 1	
Introduction	1
1.1. Purpose of the Study	1
1.2. Roadmap of the Study	2
1.3. Importance of the Study	2
1.4. Features of the ECR-MW-CVD System Used in this Study	3
1.5. Other Components of Interest of the Study	4
1.5.1. Features of the Films Deposited in the Study	4
1.5.2. The Deposition of Hydrocarbon Films	5
1.5.3. The Verification-by-Proof Cause-and-Effect Phase	6
1.6. Overview of the Relationship between the ECR-MW-CVD Method, its Ambipolar-State's Character, and the Properties of Vapor Deposited Films	7

Table of Contents (Continue)

	1.7. The Rest of this Manuscript	9
	1.8. References	10
Chapter 2	The Electron Cyclotron Resonance – Microwave – Chemical Vapor Deposition or (ECR-MW-CVD) Method and Its Ambipolar-State's Character	13
	2.1. A Justification to Depict the Ambipolar-State's Character of the ECR-MW-CVD Method	13
	2.2. A History behind Vapor Deposition and Characterization of Hydrocarbon Films	16
	2.2.1. Vapor Deposition of Hydrocarbon Films using Non-ECR-MW Sources	16
	2.2.2. Vapor Deposition of Hydrocarbon Films using the ECR-MW-CVD Method	17
	2.2.3. Characterization of Vapor-Deposited Hydrocarbon Films	20
	2.2.4. Exploring the ECR-MW-CVD Method for making Capsules for Laser Fusion Experiments	21
	2.3. Current Knowledge about Growth Models and Properties of Films made using Vapor Deposition Methods	22
	2.4. Current Knowledge about the ECR-MW Source and the ECR-MW Plasma Environment	25
	2.5. Other Aspects to Consider when Using an ECR-MW-CVD Source for Vapor-Depositing Hydrocarbon Films	28
	2.6. The Principles Governing the Science of an ECR-MW-CVD Method	31
	2.7. Understanding the Concept 'Ambipolar-State' and the Ambipolar-State's Character of an ECR-MW-CVD Method	35
	2.7.1. Landing on the Concept 'Ambipolar-State'	35

Table of Contents (Continue)

	2.7.2. Defining the Concept Ambipolar-State	37
	2.7.3. The Intrinsic Nature of the Ambipolar-State's Character of an ECR-MW-CVD Method and Its Influence in the Properties of Hydrocarbon Films	39
	2.8. The Forced Nature of the Ambipolar-State's Character of the ECR-MW-CVD Method	44
	2.8.1. Effect of Power and Resistance of an ECR-MW Source on the Ambipolar-State's Character of the ECR-MW-CVD Method and Its Influence in the Properties of Hydrocarbon Films	45
	2.8.2. The Effects that Thermal or Electrical Heating of the Substrates has on the Ambipolar-State's Character of the ECR-MW-CVD Method and Its Influence in the Properties of Hydrocarbon Films	48
	2.9. Probing that the Ambipolar-State's Character of the ECR-MW-CVD Method can be Depicted	49
	2.10. References	50
Chapter 3	The Details of the Experimentation behind the Depiction of the Ambipolar-State's Character of the ECR-MW-CVD Method	63
	3.1. Overview of the Third Chapter	63
	PART I – Commissioning and Characterizing the ECR-MW-CVD System	64
	3.2. Commissioning the ECR-MW-CVD System	64
	3.2.1. Details about the Assembly of the ECR-MW-CVD System	64

Table of Contents (Continue)

3.2.2. Handling and Flowing the Gases inside the ECR-MW-CVD System	65
3.2.3. Operational Details about the ECR-MW Source	65
3.2.4. Operational Details about the Substrates Heater	66
3.2.5. Operational Details about the Direct Voltage Discharge Apparatus	68
3.3. Testing the ECR-MW-CVD System	68
3.3.1. Inspecting the Operational Integrity of the ECR-MW-CVD System	69
3.3.2. Testing the ECR-MW-CVD System in Operation	69
3.3.2.1. Observation of the Pressure-over-Flow Rate Curves of the Gases	69
3.3.2.2. Observation of the Susceptibility of the Gases in Response to the ECR-MW Source	70
3.3.2.3. Observation of the Pressure over Temperature Flow Regime Diagrams Generated using the Reciprocal Knudsen Number as Regime Criteria	72
PART II – Depositing and Characterizing Hydrocarbon Films	74
3.4. The Strategy behind the Deposition of Hydrocarbon Films	74
3.5. The Strategy for Characterizing Hydrocarbon Films	75
3.5.1. Measuring the Thicknesses, Determining the Coating Uniformities, and Observing the Microstructures of Hydrocarbon Films	76

Table of Contents (Continue)

	3.5.2. Determining the Densities of Hydrocarbon Films	77
	3.5.3. Determining the Toughness of Hydrocarbon Films	80
	3.5.4. Observing the Refractive Indices, Colors, Translucencies, and Surface Chemistries of Hydrocarbon Films	80
	3.6. References	85
Chapter 4	Depicting the Ambipolar-State's Character of the ECR-MW-CVD Method through Observations on the Properties of Hydrocarbon Films	93
	4.1. Strengthening the Knowledge Gotten on the Second Chapter and Complementing the Depiction of the Ambipolar-State's Character of the ECR-MW-CVD Through Observations made on Hydrocarbon Films	93
	PART I. Relating the Ambipolar-State's Character of the ECR-MW-CVD Method and Films' Properties using One Process Variable	95
	4.2. Observations on Films Deposited at Different Times	95
	4.3. Observations on Films Deposited Settling the ECR-MW Source at Different Powers and Resistances	101
	4.3.1. Observations on Films Deposited at Different Powers	101
	4.3.2. Observations on Films Deposited at Different Resistances	103
	4.4. Observations on Films Deposited on Thermally and Electrically Heated Substrates	104
	4.4.1. Observations on Films Deposited on Thermally Heated Substrates	105
	4.4.2. Observations on Films Deposited on Electrically Heated Substrates	106

Table of Contents (Continue)

	PART II. Relating Multiple Films' Properties to the Ambipolar-State's Character of the ECR-MW-CVD Method in Selected Samples	108
	4.5. Observing Multiple Properties of Hydrocarbon Films in Selected Samples	108
	4.5.1. Observations on the Refractive Indices, Colors, Translucencies, and Thicknesses of Hydrocarbon Films	109
	4.5.2. Observations on the Refractive Indices, Colors, Translucencies, and Surface Chemistries of Hydrocarbon Films	111
	4.5.3. Observations on the Surface Chemistry and Microstructure of Hydrocarbon Films	114
	4.5.4. Observations on the Thickness and Coating Uniformity of Hydrocarbon Films	116
	4.5.5. Observations on the Roughness of Hydrocarbon Films	116
	4.5.6. Relating the Ambipolar-State's Character of the ECR-MW-CVD Method to the Energy Per Molecule of the ECR-MW-CVD System and the Microstructure of Hydrocarbon Films	118
	4.6. References	121
Chapter 5	Concluding Remarks and Recommendations for Future Studies	124
	5.1. Implications of the Study	124
	5.2. Postulates Based on the Current Knowledge of the Ambipolar-State's Character of the ECR-MW-CVD Method	126
	5.3. Using the Knowledge Provided by the Ambipolar-State's Character of the ECR-MW-CVD Method to Fulfill the Needs of the Fusion Community	127

Table of Contents (Continue)

	5.4. Expanding the Knowledge of the Ambipolar-State's Character of the ECR-MW-CVD Method Beyond the Scope of Fusion Sciences	128
	5.5. A process to Build More Knowledge from the Concept 'Ambipolar-State' and the Current Status of the Knowledge about the Ambipolar-State's Character of the ECR-MW-CVD's Method	132
	5.6. References	134
Appendix A	Creating the Reciprocal Knudsen Number Flow Regime Curves for Air and Methane Inside an Electron Cyclotron Resonance – Microwave – Chemical Vapor Deposition System at Specific Ranges of Gas Pressures and Temperatures	137
	A.1. About Appendix A	137
	A.2. The Reciprocal Knudsen Number	138
	A.3. The Mean Free Path	138
	A.4. Creating the RKN Flow Regime Curves	140
	A.5. References	143
Appendix B	Determination of the Density of Hydrocarbon Films and Silicon Substrates of Different Sizes	146
	B.1. About Appendix B	146
	B.2. Density	146
	B.3. Determination of the Density of Silicon Substrates of Different Sizes	147
	B.4. References	150
Appendix C	Matching Ellipsometry Data using Cauchy's Layer Model by Means of the Mean Squared Error (MSE) Statistical Approximation Method	151
	C.1. About Appendix C	151
	C.2. The Cauchy's Layer Model	151

Table of Contents (Continue)

	C.3. Matching Up the Mean Thickness of Film Grown at Different Powers, and the Cauchy's Layer Model via the Mean Squared Error (MSE) Method	152
	C.4. References	154
Appendix D	Illustrating the Use of the Integration and Peak Area Measurement Method to Determine the Fractions of Carbon sp, sp ² , and sp ³ Hybridized Bonds in a Hydrocarbon Film Sample Using Raman Spectroscopy	155
	D.1. About Appendix D	155
	D.2. Using Raman Spectroscopy to Determine the Amount of Carbon sp, sp ² , and sp ³ Hybridized Bonds in Hydrocarbon Films Samples	155
	D.3. The Integration and Peak Area Measurement Method	157
	D.4. Illustrating the Use of the Integration and Peak Area Measurement Method for the Case in which a Hydrocarbon Film Sample is Prepared via ECR-MW-CVD in 1d at 200 W using 4 Pa of Methane	159
	D.5. References	162
Appendix E	Observations on Hydrocarbon Films Deposited at Different Times by means of Electron Cyclotron Resonance – Microwave – Chemical Vapor Deposition (ECR-MW-CVD)	165
	E.1. About Appendix E	165
	E.2. Observations on Hydrocarbon Films Deposited at Different Times Adjusting the Power of the ECR-MW Source to 200 W	166
	E.3. Observations on Hydrocarbon Films Deposited at Different Times Adjusting the Power of the ECR-MW Source to 500 W	168
	E.4. Observations on Hydrocarbon Films Deposited at Different Times Adjusting the Power of the ECR-MW Source at 200 and 500 W	170

Table of Contents (Continue)

Appendix F	Observations on Hydrocarbon Films Deposited Adjusting the Electron Cyclotron Resonance – Microwave (ECR-MW) Source to Different Powers	171
	F.1. About Appendix F	171
	F.2. Observations on Hydrocarbon Films Deposited Adjusting the ECR-MW Source to Different Powers	172
Appendix G	Observations on Hydrocarbon Films Deposited Adjusting the Electron Cyclotron Resonance – Microwave (ECR-MW) Source to Different Resistances	175
	G.1. About Appendix G	175
	G.2. Observations on Hydrocarbon Films Deposited Adjusting the ECR-MW Source to Different Resistances	176
Appendix H	Observations on Hydrocarbon Films Deposited on Thermally Heated Substrates	179
	H.1. About Appendix H	179
	H.2. Observations on Hydrocarbon Films Deposited on Thermally Heated Substrates	180
Appendix I	Observations on Hydrocarbon Films Deposited on Electrically Heated Substrates	182
	I.1. About Appendix I	182
	I.2. Observations on Hydrocarbon Films Deposited on Electrically Heated Substrates	183
	Glossary of Terms	186
	Bibliography	202

Biographical Sketch

Jesús M. García-Figueroa — Jesús — obtained a master's of engineering in chemical engineering at the University of Puerto Rico–Mayaguez in 2012. He did a double bachelor's degree in chemistry and chemical engineering and a minor in manufacturing, management, and business technology enterprises at the University of Puerto Rico–Mayaguez in 2009. His most recent contribution is the first depiction of the ambipolar-state of the electron cyclotron resonance – microwave – chemical vapor deposition (ECR-MW-CVD) method. He also was the first to analyze the costs of a local bioproducts processing plant using microalgae biomass as feedstock at the detailed design level. His projects have been sponsored by the Air Force Research Laboratories, the American Institute of Chemical Engineers, the American Nuclear Society, Bristol Myers Squibb, the MasterCard Foundation, the National Science Foundation, the Sloan Foundation, the University of Puerto Rico, the University of Rochester, the U.S. Department of Defense, the U.S. Department of Education, and the U.S. Department of Energy. Jesús' interests are engineering, enterprises, sciences, management, and technology, and connect processes and their products through the virtues of the scientific method.

Publications:

1. García-Figueroa JM, Harding DR. Relationship between the Gas-Phase Reactions Occurring within an Electron Cyclotron Resonance- (ECR) Microwave- (MW) CVD Process and the Properties of Hydrocarbon Films. PowerPoint presented: 2019 MRS Fall Meeting & Exhibit; December 1-6, 2019; Boston, Massachusetts, United States of America. Available from: García-Figueroa's website at: <https://inquchild09.wixsite.com/inquchild09/in-rochester>.

2. García-Figueroa JM, Harding DR. Effect of High Ion and Electron Densities and Substrate Temperature on the Properties of Glow-Discharge-Polymer Films. Poster presented at 22nd Target Fabrication Conference; March 12-16, 2017; Nevada National Security Site, Nevada, United States of America. Available from: García-Figueroa's website at: <https://inquchild09.wixsite.com/inquchild09/in-rochester>.

Abstract

The content of this study provides evidence of the non-collisional, transient, discrete, discriminant, and susceptible nature of the electron cyclotron resonance — microwave — chemical vapor deposition (ECR-MW-CVD) method ambipolar-state's character, its relationship to the processing conditions in an ECR-MW-CVD system, and its influence over the properties of hydrocarbon films. More important, the results of this study qualify the ECR-MW-CVD method for upgrading shells for laser fusion experiments at $\leq 200^{\circ}\text{C}$ and provide first-hand knowledge of how to use the ECR-MW-CVD method ambipolar-state's character to deposit specialty types of hydrocarbon films. In this study, hydrocarbon films were deposited on silicon substrates using a home-built ECR-MW-CVD system, methane, and hydrogen and were characterized via x-ray, Raman, and Fourier transform infrared spectroscopies, scanning electron and probe microscopies, photography, nano-indentation, gravimetry, ellipsometry, and 1-D measurements. Beyond dissecting the ECR-MW-CVD method ambipolar-state's character and uncovering its role in dictating the properties of hydrocarbon films deposited in an ECR-MW-CVD system, this study concludes by suggesting ways to keep exploring aspects from the concept 'ambipolar-state' of the ECR-MW-CVD method for the benefit of humanity.

Contributors and Funding Sources

Committee Chair

Professor Melissa Sturge-Apple | University of Rochester

Thesis Supervisor

Professor David R. Harding | University of Rochester

Committee Members

Professor Mitchell Anthamatten | University of Rochester

Professor Wyatt E. Tenhaeff | University of Rochester

Professor Jennifer D. T. Kruschwitz | University of Rochester

Funding Sources and Disclaimer

The work on this thesis was supported by the Department of Energy National Nuclear Security Administration under Award Number DE-NA0003856, the University of Rochester, and the New York State Energy Research and Development Authority. Nonetheless, its content, expressions, and views are the author's sole responsibility.

List of Tables

Tables Shown in Chapter 2

Table	Caption	Page
2.5-1	Electron densities, ionization energies, and mean kinetic temperatures inside HDR (helical discharge resonance), ECR-MW-CVD (electron cyclotron resonance – microwave – chemical vapor deposition), and PA-CVD (plasma assisted chemical vapor deposition) systems ^{2, 9, 13, 16, 79, 80 – 82, 87} .	31
2.7.1-1	Electron densities, ionization frequencies, and conductivities inside HDR (helical discharge resonance), ECR-MW-CVD (electron cyclotron resonance – microwave – chemical vapor deposition), and PA-CVD (plasma assisted chemical vapor deposition) environments ^{2, 9, 13, 16, 79, 81, 85, 87, 93 – 95} .	36

Tables Shown in Chapter 3

Table	Caption	Page
3.4-1	Summary of conditions used to vapor-deposit hydrocarbon films.	74
3.5-1	Summary of techniques used to characterize films by category.	75

List of Tables (Continue)

Tables Shown in Appendix A

Table	Caption	Page
A.4-1	RKNs for Air at Specific Pressures and Temperatures ^{2, 3} .	141
A.4-2	RKNs for Methane at Specific Pressures and Temperatures ^{2, 3} .	142
A.4-3	Data of Flow Regime Curves for Air Inside an ECR-MW-CVD System (L = 0.1016 m).	143
A.4.4	Data of Flow Regime Curves for Methane Inside an ECR-MW-CVD System (L = 0.1016 m).	143

Tables Shown in Appendix B

Table	Caption	Page
B.3-1	Dimensions, nominal areas, and volumes of the substrates used in the study. The nominal thickness of each substrate was 0.38 mm ^{1, 5, 8} .	148
B.3-2	Nominal areas and individual masses of the substrates used in the study.	148
B.3-3	Nominal areas, mean masses, and mass-standard deviations of the substrates used in the study ² .	149
B.3-4	Nominal areas, mean densities, and accuracy percentages of the substrates used in the study. The theoretical value of density for silicon substrates is 2.329 g/cm ³ ^{1, 2, 5-8} .	149

Tables Shown in Appendix C

Table	Caption	Page
C.3-1	Cauchy's layers model constant coefficients for films deposited at different powers. Each deposition was done in 1d using 4 Pa of methane.	153
C.3-2	Mean thicknesses and mean squared error (MSE) values for films deposited at different powers. Each deposition was done in 1d using 4 Pa of methane.	153

List of Tables (Continue)

Tables Shown in Appendix D

Table	Caption	Page
D.4-1	Observations on the geometrical shapes for the peak in Figure D.4-1 a).	161
D.4-2	Observations on the geometrical shapes for the peak in Figure D.4-1 b).	161
D.4-3	Observations on the geometrical shapes for the peak in Figure D.4-1 c).	161
D.4-4	Observations on the geometrical shapes for the peak in Figure D.4-1 d).	161
D.4-5	Summary of areas observed in Figure D.4-1.	162

Tables Shown in Appendix E

Table	Caption	Page
E.2-1	Summary of conditions used to deposit hydrocarbon films. Each film was deposited at different times adjusting the power of the ECR-MW source to 200 W.	166
E.2-2	Coating uniformities of hydrocarbon films deposited on substrate II — the piece used to determine the density of the film — at different times, adjusting the power of the ECR-MW source to 200 W.	166
E.2-3	Coating uniformities of hydrocarbon films deposited on substrate I — the piece used to observe the film's toughness — at different times, adjusting the power of the ECR-MW source to 200 W.	167
E.2-4	Percentages of difference between the thicknesses of hydrocarbon films deposited on substrates I and II. Each deposition was done at different times, adjusting the power of the ECR-MW source to 200W.	167
E.2-5	Roughnesses of hydrocarbon films deposited on substrate III. Each film was deposited at different times, adjusting the power of the ECR-MW source to 200 W. The area scanned was 100 μm^2 .	167
E.2-6	Roughnesses of hydrocarbon films deposited on substrate III. Each film was deposited at different times, adjusting the power of the ECR-MW source to 200 W. The area scanned was 10,000 μm^2 .	167

List of Tables (Continue)

Tables Shown in Appendix E (*Continue*)

Table	Caption	Page
E.3-1	Summary of conditions used to deposit hydrocarbon films. Each film was deposited at different times, adjusting the power of the ECR-MW source to 500 W.	168
E.3-2	Coating uniformities of hydrocarbon films deposited on substrate II — the piece used to determine the density of the film — at different times, adjusting the power of the ECR-MW source to 500 W.	168
E.3-3	Coating uniformities of hydrocarbon films deposited on the substrate I — the piece used to observe the film's toughness — at different times, adjusting the power of the ECR-MW source to 500 W.	168
E.3-4	Percentages of difference between the thicknesses of hydrocarbon films deposited on substrates I and II. Each deposition was done at different times adjusting the power of the ECR-MW source to 500W.	169
E.3-5	Roughnesses of hydrocarbon films deposited on substrate III. Each film was deposited at different times, adjusting the power of the ECR-MW source to 500 W. The area scanned was 100 μm^2 .	169
E>3-6	Roughnesses of hydrocarbon films deposited on substrate III. Each film was deposited at different times, adjusting the power of the ECR-MW source to 500 W. The area scanned was 10,000 μm^2 .	169
E.4-1	Average densities of hydrocarbon films deposited at 200 and 500. Densities were calculated using Equation B.2-2.	170
E.4-2	The toughness of hydrocarbon films deposited at 200 and 500 W determined using nano-indentation as described in Section 3.5.3.	170

List of Tables (Continue)

Tables Shown in Appendix F

Table	Caption	Page
F.2-1	Summary of operational conditions used to deposit hydrocarbon films at different powers.	172
F.2-2	Coating uniformities of hydrocarbon films deposited on substrate II — the piece used to determine the density of the film — at different powers.	172
F.2-3	Coating uniformities of hydrocarbon films deposited on substrate I — the piece used to observe the toughness of the film — at different powers.	173
F.2-4	Percentages of difference between the thicknesses of hydrocarbon films deposited at different powers on substrates I and II.	173
F.2-5	Densities and toughness of hydrocarbon films deposited at different powers.	173
F.2-6	Roughnesses of hydrocarbon films deposited at different powers on substrate III. The area scanned was 100 μm^2 .	173
F.2-7	Roughnesses of hydrocarbon films deposited at different powers on substrate III. The area scanned was 10,000 μm^2 .	174
F.2-8	Refractive indices, colors, and translucencies of hydrocarbon films deposited at different powers on substrate IV.	174
F.2-9	Percentages of carbon sp, sp ² , and sp ³ hybridized bonds in hydrocarbon films deposited at different powers on substrate IV.	174

List of Tables (Continue)

Tables Shown in Appendix G

Table	Caption	Page
G.2-1	Summary of operational conditions used to deposit hydrocarbon films adjusting the resistance of the ECR-MW source at different values.	176
G.2-2	Coating uniformities of hydrocarbon films deposited on substrate II — the piece used to determine the density of the film — by adjusting the ECR-MW source at different resistances.	176
G.2-3	Coating uniformities of hydrocarbon films deposited on substrate I — the piece used to observe the film's toughness — by adjusting the ECR-MW source at different resistances.	177
G.2-4	Percentages of difference between the thicknesses of hydrocarbon films deposited on substrates I and II by adjusting the ECR-MW source at different resistances.	177
G.2-5	Roughnesses of hydrocarbon films deposited on substrate III by adjusting the ECR-MW source at different resistances. The area scanned was 100 μm^2 .	177
G.2-6	Roughnesses of hydrocarbon films deposited on substrate III by adjusting the ECR-MW source at different resistances. The area scanned was 10,000 μm^2 .	177
G.2-7	Densities and toughness of hydrocarbon films deposited by adjusting the ECR-MW source at different resistances.	178

List of Tables (Continue)

Tables Shown in Appendix H

Table	Caption	Page
H.2-1	Summary of operational conditions used to deposit hydrocarbon films on thermally heated substrates.	180
H.2-2	Coating uniformities of hydrocarbon films deposited on substrate II — the piece used to determine the density of the film — on thermally heated substrates.	180
H.2-3	Coating uniformities of hydrocarbon films deposited on substrate I — the piece used to observe the film's toughness — on thermally heated substrates.	180
H.2-4	Percentages of difference between the thicknesses of hydrocarbon films deposited on substrates I and II on thermally heated substrates.	181
H.2-5	Roughnesses of hydrocarbon films deposited on substrate III on thermally heated substrates. The area scanned was 100 μm^2 .	181
H.2-6	Roughnesses of hydrocarbon films deposited on substrate III on thermally heated substrates. The area scanned was 10,000 μm^2 .	181
H.2-7	Densities and toughness of hydrocarbon films deposited on thermally heated substrates.	181

List of Tables (Continue)

Tables Shown in Appendix I

Table	Caption	Page
I.2-1	Summary of operational conditions used to deposit hydrocarbon films on electrically heated substrates.	183
I.2-2	Coating uniformities of hydrocarbon films deposited on substrate II — the piece used to determine the density of the film — on electrically heated substrates.	183
I.2-3	Coating uniformities of hydrocarbon films deposited on substrate I — the piece used to observe the toughness of the film — on electrically heated substrates.	184
I.2-4	Percentages of difference between the thicknesses of hydrocarbon films deposited on substrates I and II on electrically heated substrates.	184
I.2-5	Roughnesses of hydrocarbon films deposited on substrate III on electrically heated substrates. The area scanned was 100 μm^2 .	185
I.2-6	Roughnesses of hydrocarbon films deposited on substrate III on electrically heated substrates. The area scanned was 10,000 μm^2 .	185
I.2-7	Densities and toughness of hydrocarbon films deposited on electrically heated substrates.	185

List of Figures

Figures Shown in Chapter 1

Figure	Caption	Page
1.6-1	Atomic transfer phenomena happening in VD methods ¹⁷ .	7

Figures Shown in Chapter 2

Figure	Caption	Page
2.4-1	Deposition of species inside an ECR-MW-CVD system.	26
2.5-1	Species generated inside an ECR-MW-CVD system using methane ^{13, 16, 79, 86} . The term '1 st ionization energy' refers to the energy needed to start ionizing a specie.	29
2.7.1-1	Illustration of the ambipolar-state of the ECR-MW-CVD method at the gas-substrate interphase in two dimensions. The circles demarcate the more and less electrophilic species. Where the term 'more electrophilic' distinguish species such as electrons or partially negative ions from the species demarcated with the term 'less electrophilic' such as neutrally charged particles or positive charged ions. The curved lines demarcate the end the Debye sheath; and the measuring line demarcates the Debye lengths between species.	37

List of Figures (Continue)

Figures Shown in Chapter 2 (*Continue*)

Figure	Caption	Page
2.7.3-1	Depiction of a film growing inside an <i>ECR-MW</i> system. a) and b) show a film growing as layer-over-layer due to the interaction between more electrophilic species in the interphase and the substrate's surface; c) and d) show islands forming on top of the crescent layers of a film due to the relative interaction between more and less electrophilic species ^{12, 78} .	42
2.8.1-1	Decomposition of two molecules of methane exposed to high power or low resistance (Δ) ^{16, 79, 80, 85, 86} . I, two molecules of methane decomposing to form hydron and ethene; II, ethene decomposing to form hydron and ethyne; III, ethyne decomposing to form hydron and a carbon-carbon -yne specie.	47

Figures Shown in Chapter 3

Figure	Caption	Page
3.2.1-1	One-line diagram of the <i>ECR-MW-CVD</i> system's assembly. Dashed lines indicate material flow. Objects are identified using solid lines.	64
3.2.4-1	Detail top, a), and front, b), view diagrams of the substrates heater's armor.	67
3.2.5-1	One-line diagram of the substrates' direct voltage discharge apparatus.	68
3.3.2.1-1	Pressure over gas flow rate curves for methane and hydrogen using a turbo-molecular pump, a), and a rotary-vane pump, b). The points on these graphs were measured by flowing the gas on test for thirty minutes with the valve fully open at standard room temperature and humidity conditions.	70
3.3.2.2-1	Gas pressure in response to the electron cyclotron resonance microwave power. The alphanumeric characters "Ar," "H2," and "CH4" are used to identify argon, hydrogen, and methane. Each gas was flowed individually at ten sccm for one minute.	71

List of Figures (Continue)

Figures Shown in Chapter 3 (*Continue*)

Figure	Caption	Page
3.3.2.3-1	Pressure over temperature flow regime diagrams based on the reciprocal Knudsen number (RKN) for air, (a), and methane, (b) ^{39, 41} . The data was gathered from the National Institute of Standards and Technology ^{47, 48} and adjusted to the system's characteristic length, which is 101.6 millimeters ⁴⁸ . The words "VISCOUS," "TRANSITION," and "MOLECULAR" demarcate the type of flow regime. The details of how these diagrams were generated are discussed in the Appendix A.	73
3.5-1	Detail diagram that shows how substrates were positioned on top of the substrate's holder. The nominal dimensions of substrates I, II, III, and IV were 40 mm-height and 10 mm-width, 5 mm-height and 5 mm-width, 5 mm-height and 5 mm-width, and 40 mm-height and 20 mm-width. All substrates were 0.38 mm thick.	76
3.5.1-1	Observations of on bare substrates acquired using scanning electron and scanning probe microscopies at 60° and 55° respectively. a), c), and e) are scanning probe microscopy images of 8.75, 10 x 10 ⁻³ , 0.1 x 10 ⁻³ square-millimeters samples. b), d), and f) are scanning electron microscopy images of 1.27, 0.950 x 10 ⁻⁶ , and 2.78 x 10 ⁻⁶ square-millimeters samples. The intrinsic defects on the substrates are circled on a).	78
3.5.2-1	Calibration of substrates II and III. a) shows a picture of the substrates by size. b), c), and d) show the mean density, its accuracy, and the mean weight for each substrate by size respectively. The values above the black line in b) and c) represent the theoretical density of pure silicon, 2.329 g/cm ³ , which is equal to an accuracy of 100%. Details of how b), c), and d) were generated are discussed in the Appendix B.	79
3.5.4-1	Ellipsometry data of films deposited at 650 W. The film was deposited in one day using 4 Pa of methane. The beam's incidence angle was 75.5°. The 1 st and 2 nd datasets demarcate the experimental and modeled results which were gathered from the same sample revolved at 180° and in parallel to the sample's plate at a wavelength of 533 nm. Each film's refractive index was obtained as described in Appendix C.	81

List of Figures (Continue)

Figures Shown in Chapter 3 (*Continue*)

Figure	Caption	Page
3.5.4-2	Illustration of how the translucencies — and optionally, colors — of films were ascertained. A, B, and C are boolean expressions ⁷² . A and B are obtained via telephotography at 90°. C was computed using a closed source presentation software ^{63–67} .	82
3.5.4-3	Grazing-angle Fourier transform infrared and Raman spectrums of films deposited at different powers. All the films were deposited in one day using 4 Pa of methane.	83
3.5.4-4	Fractions of hybridized carbon bonds for films deposited at different powers. The fractions were calculated employing the integration and peak area measurement method ⁷³ on data gathered via Raman spectroscopy as illustrated in Appendix D. The films were deposited in one day using 4 Pa of methane. The percentages of each hybridized bond were calculated by multiplying the fraction of each hybridized carbon bond by 100.	84

Figures Shown in Chapter 4

Figure	Caption	Page
4.2-1	Scanning electron microscopy images of films deposited at different times. The images shown in a) were obtained from films deposited at 200 W. The images shown in b) were obtained from films deposited at 500 W. Each film was deposited using 4 Pa of methane. Each image has an area of 200 μm^2 .	97
4.2-2	Scanning probe microscopy images, a), and scanning electron microscopy images, b), of films deposited at different times. Each film was deposited at 200 W using 4 Pa of methane. Each image in a) has an area of 10,000 μm^2 . The area of each image in b) is noted right next to the bottom of the image.	98

List of Figures (Continue)

Figures Shown in Chapter 4 (*Continue*)

Figure	Caption	Page
4.2-3	Mean densities and thicknesses of films deposited at different times. The data shown in a) and c) was gathered from films deposited at 200 W. The data shown in b) and d) was gathered from films deposited at 500 W. Each film was deposited using 4 Pa of methane. The percentage of variance between measurements of the same sample was not greater than 6%. The percentage of deviation between measurements in two different samples was not greater than 5%.	99
4.2-4	Mean stresses, hardnesses, and thicknesses of films deposited at different times. The data shown in a), c), and e) was obtained from films deposited at 200 W. The data shown in b), d), and f) was obtained from films deposited at 500 W. Each film was deposited using 4 Pa of methane. The percentage of variance between measurements of the same sample was not greater than 6%. The percentage of deviation between measurements in two different samples was not greater than 5%.	100
4.3.1-1	Scanning electron microscopy images of films deposited at different powers. Each film was deposited in 1d using 4 Pa of methane and each image has an area of 50 μm^2 .	102
4.3.1-2	Mean densities, a), and thicknesses, b), of films deposited at different powers. Each film was deposited in 1d using 4 Pa of methane.	103
4.3.2-1	Scanning electron microscopy images, a), and mean thicknesses, b), of films deposited at different ECR-MW resistances. Each film was deposited for 1day at 500 W using 4 Pa of methane. Each image has an area of 50 μm^2 . The word 'Density' demarcates the pieces used to measure the mean densities of the films. The word 'Toughness' demarcates the pieces used to measure the mean stresses and hardnesses of the films.	104

List of Figures (Continue)

Figures Shown in Chapter 4 (*Continue*)

Figure	Caption	Page
4.4.1-1	Scanning electron microscopy images, a), and mean thicknesses, b), of films deposited at different temperatures. The data at 120°C and 200°C was obtained from films deposited on thermally heated substrates. Each film was deposited using methane diluted in hydrogen at a pressure of 4 Pa. Each image has an area of 200 μm^2 . The word 'Density' demarcates the pieces used to measure the mean densities of the films. The word 'Toughness' demarcates the pieces used to measure the mean stresses and hardnesses of the films.	106
4.4.2-1	Scanning electron microscopy images of films deposited on electrically heated substrates. Each film was deposited in 6hrs using 4 Pa of methane. The images shown in a) were obtained from films deposited at 100 W. The images shown in b) were obtained from films deposited at 500 W. Each image has an area of 200 μm^2 .	107
4.4.2-2	Mean thicknesses of films deposited over electrically heated substrates. The data shown in a), b), c) and d) was gathered from films deposited at 100 W, 200 W, 350 W and 500 W. Each film was deposited in 6hrs using 4 Pa of methane. The word 'Density' demarcates the pieces used to measure the mean densities of the films. The word 'Toughness' demarcates the pieces to measure the mean stresses and hardnesses of the films.	108
4.5.1-1	Refractive indices, a), % of translucencies and colors, b), and mean thicknesses, c), of films deposited at different powers. Each film was deposited in 1d using 4 Pa of methane.	110
4.5.2-1	Refractive indices, a), % of translucencies and colors, b), and deconvolution of bonds, c) and d), of films deposited at different powers. Each film was deposited in 1d using 4 Pa of methane.	113

List of Figures (Continue)

Figures Shown in Chapter 4 (*Continue*)

Figure	Caption	Page
4.5.3-1	Scanning electron microscopy images and x-ray photoelectron spectroscopy graphs of films deposited at different powers and temperatures. Each image has a width of 10 μm and an area of 200 μm^2 . Each film was deposited in 1hr at 4 Pa using a mixture of 20:80 methane:hydrogen. The data shown in b) and c) was gathered from films deposited on thermally heated substrates. The mean thicknesses of the film in a), b) and c) are 1.1 μm , 1.1 μm and 0.5 μm .	115
4.5.6-1	Scanning electron microscopy images, a), and mean thicknesses, b), of films deposited at different pressures. Each film was deposited in 1d using methane. Each image has an area of 50 μm^2 . The word 'Density' demarcates the pieces used to measure the mean densities of the films. The word 'Toughness' demarcates the pieces used to measure the mean stresses and hardnesses of the films.	119
4.5.6-2	Scanning electron microscopy images, a), and mean thicknesses, b), of films deposited at different percentages of methane diluted in hydrogen. Each film was deposited in 1d. Each image has an area of 200 μm^2 . The word 'Density' demarcates the pieces used to measure the mean densities of the films. The word 'Toughness' demarcates the pieces used to measure the mean stresses and hardnesses of the films.	120

Figures Shown in Appendix D

Figure	Caption	Page
D.4-1	Raman peaks identified according to the integration and peak area measurement method ^{12, 13, 15} for a spectrograph of hydrocarbon film sample prepared via ECR-MW-CVD in 1d, at 200 W using 4 Pa of methane. The horizontal dashed lines demarcate the boundary between carbon sp^3 , sp^2 , and sp hybridized bonds. The vertical dashed line demarcates the scale of five points in the peaks' intensity. The roman numbers designate the elements — shapes traced by gray lines — under each peak. The blank was cyclohexane at 17°C ³ .	160

List of Equations

Equations Shown in Chapter 2

Equation	Caption	Page
2.6-1	The Newton's 2nd Law.	31
2.6-2	The Lorentz Law.	32
2.6-3	Combination of the Newton's 2nd Law and the Lorentz Law.	32
2.6-4	Derived Expression for the Electron's Speed Inside the ECR-MW Source's Electric field.	33
2.6-5	Mathematical Expression for the Gyration Radius Inside an ECR-MW Plasma.	33
2.6-6	Characteristic Equation for Designing an ECR-MW Source.	33
2.6-7	Gyration Radius of an Electron Exposed to a Magnetic Field.	34
2.6-8	The Electron's Gyration Frequency in Hz.	34
2.7.1-1	Scalar Conductivity for Magnetized Non-thermal Plasmas	36

Equations Shown in Appendix A

Equation	Caption	Page
A.2-1	The Reciprocal Knudsen Number (RKN).	138
A.3-1	The Gibbs Phase Rule.	138
A.3-2	Mean Free Path Adjusted for an ECR-MW-CVD System.	140
A.4-1	The Double Interpolation Equation to Determine Pressure Using Values of Temperature and RKN.	142

List of Equations (Continue)

Equations Shown in Appendix B

Equation	Caption	Page
B.2-1	Density of a Substrate.	146
B.2-2	Density of a Film.	147

Equations Shown in Appendix C

Equation	Caption	Page
C.2-1	The Cauchy's Layer Model.	151

Equations Shown in Appendix D

Equation	Caption	Page
D.3-1	The Area of a Triangle.	157
D.3-2	The Area of a Square.	157
D.3-3	Total Area of Carbon sp, sp ² , and sp ³ Hybridized Bonds.	157
D.3-4	Fraction of Carbon sp Hybridized Bonds.	158
D.3-5	Fraction of Carbon sp ² Hybridized Bonds.	158
D.3-6	Fraction of Carbon sp ³ Hybridized Bonds.	158

List of Symbols

Symbols Shown in Chapter 2

Symbol	Name	Unit
σ_s	Plasma's Conductivity	S/m
B_x	Magnetic Field	Ns/m or Gauss
dv_e/dt	Acceleration of the Electron or Electron's Velocity Rate	m/s ²
e^2	Elementary Charge Unit equal to 1.602×10^{-19}	C
$E_{ }$	Electric Field	N/C
f_{ce}	ECR-MW Source's Oscillation Frequency	Hz
F_e	Force of Moving Electron	N
m_e	Electron's Mass, equal to 9.109×10^{-31}	kg
n_e	Electron's Density of the Plasma	m ⁻³
Q	Electron's Charge	C
Q/m_e	1.758×10^{11}	C/kg
V	Ionization Potential	eV or Volts
v_e	Electron's Velocity	m/s
r_e	Electron's Gyration Radius	m or mm

List of Symbols (Continue)

Symbols Shown in Appendix A

Symbol	Name	Unit
Com	Number of Compounds	—
Kn^{-1}	The Reciprocal Knudsen Number (RKN)	—
F	Degrees of Freedom	—
L	Characteristic Length of the ECR-MW-CVD System, 0.1016.	m
λ	Mean Free Path	m
μ	Viscosity	Pa-s
M	Molecular Weight	g/mol
P	Pressure	Pa
P_x	Pressure in the Point x	Pa
P_1	Pressure in the Point 1	Pa
P_2	Pressure in the Point 2	Pa
Ph	Number of Phases	—
R	Gas Constant Law, 8.314	J K ⁻¹ mol ⁻¹
RKN_x	Reciprocal Knudsen Number in the Point x	—
RKN_1	Reciprocal Knudsen Number in the Point 1	—
RKN_2	Reciprocal Knudsen Number in the Point 2	—
T	Temperature	K

Symbols Shown in Appendix B

Symbol	Name	Unit
ρ_{Film}	Density of a Film	g/cm ³
$\rho_{Substrate}$	Density of a Substrate	g/cm ³

List of Symbols (Continue)

Symbols Shown in Appendix C

Symbol	Name	Unit
A	First Coefficient of Cauchy's Layer Model	—
B	Second Coefficient of Cauchy's Layer Model	μm^2
C	Third Coefficient of Cauchy's Layer Model	μm^4
λ	Wavelength, 0.55	μm
$n(\lambda)$	Refractive Index	—

Symbols Shown in Appendix D

Symbol	Name	Unit
A_{sp}	Area of Carbon sp Hybridized Bonds	pts^2
A_{sp^2}	Area of Carbon sp^2 Hybridized Bonds	pts^2
A_{sp^3}	Area of Carbon sp^3 Hybridized Bonds	pts^2
A_{Square}	Area of a Square	pts^2
A_T	Total Area Counted in the Analysis	pts^2
A_{Triangle}	Area of a Triangle	pts^2
F_{sp}	Fraction of Carbon sp Hybridized Bonds	—
F_{sp^2}	Fraction of Carbon sp^2 Hybridized Bonds	—
F_{sp^3}	Fraction of Carbon sp^3 Hybridized Bonds	—
H	Height	pts
W	Width or Base	pts

Chapter 1

Introduction

1.1. Purpose of the Study

The study explains why and how an electron cyclotron resonance – microwave – chemical vapor deposition (ECR-MW-CVD) system was selected as a method to deposit a variety of thin films at temperatures $\leq 200^{\circ}\text{C}$ to make specific types of capsules needed for laser-fusion experiments^{1–5}. The explanation of how the unique plasma properties of the ECR feature affect the deposited-film properties is provided through the depiction of the ECR-MW-CVD method ambipolar-state's character — or sum of properties or characteristics — that define the ambipolar-state of the ECR-MW-CVD method at the gas-substrate interphase and how such ambipolar-state's character allows the molecular balance between the species that form the film at the gas-substrate interphase. The study also offers empirical evidence of how the system's processing conditions affect the ECR-MW-CVD method ambipolar-state's character and how the ECR-MW-CVD method ambipolar-state's character influences the properties of hydrocarbon films.

1.2. Roadmap of the Study

The study consists of a construction and commissioning phase, an experimentation phase, and a verification-by-proof cause-and-effect phase. The construction and commissioning phase consists of build, test, and qualify an ECR-MW-CVD system. The experimentation phase has two stages. Its first stage consists of depositing hydrocarbon films at selected conditions using the ECR-MW-CVD system. Its second stage consists of characterizing hydrocarbon films using multiple methods to determine if and how the processing variables affect the properties of the deposited films. The verification-by-proof cause-and-effect phase consists of matching the processing conditions of the system to the properties of the film using spreadsheets, images, and research literature.

1.3. Importance of the Study

Capsules containing the fuel for laser-fusion experiments must be low density and comprise of low-atomic-number elements (preferably only carbon and hydrogen), be like spheres with an out-of-round less than 0.2%, and possess higher-atomic number atoms such as silicon to help inhibit relativistic electrons from pre-heating the fuel^{2 - 6}. Most important, the surface needs to be smooth to limit Rayleigh-Taylor induced hydrodynamic instabilities from compromising the compression of the deuterium-tritium fuel to produce a high neutron yield³.

Today, these capsules are made using cylindrical inductively coupled plasma processes known as glow discharge polymerization (GDP) — processes that can vapor-deposit hydrocarbon films in a low-pressure low-thermal-equilibrium plasma. Nonetheless, there is interest in enhancing the capabilities of those GDP processes to make capsules with strength equal to or less than 200 GPa from elements with atomic-number equal to or less than 15.

An ECR-MW-CVD method might assist in the enhancement of current GDP processes by vapor-depositing hydrocarbon films on top of low-density spherical plastic shells at less than 200°C⁶⁻⁹. However, the method can not be approved for making shells until the fusion community understands how it works, why it works as it does, and how to control it to vapor-deposit desirable types of shells. Thus, this study focussed on explaining to the fusion community what types of capsules they can get through the depiction of the ECR-MW-CVD method ambipolar-state character backed up with evidence from a space parameter analysis of hydrocarbon films made at a specific condition.

1.4. Features of the ECR-MW-CVD System Used in this Study

The ECR-MW-CVD system has five main components — three of these are a vacuum chamber, a gas manifold, and a commercial ECR-MW source; the other two are a heater and DC high-voltage supply. The ECR-MW source generates waves at 2.45 GHz, the electron resonance frequency at a magnetic field of 875 Gauss^{9, 10}. The ECR-MW source heats the species inside the system by stripping electrons from the atomic species

and confining them to cyclonically motion around lines of magnetic field^{9, 10}. That type of confinement makes it possible to ionize more molecules per unit volume, or to increase the degree of ionization energy per molecule, in the system without adding thermal heat. This phenomenon allows the films to be deposited[at low temperatures⁷ with properties that otherwise only could be achieved at much higher temperatures. Nonetheless, the heater^{11, 12}, and voltage supply¹² provided supplemental heat and biased the polarity of the substrate to increase the kinetic energy of the depositing radicals^{7 – 12}.

1.5. Other Components of Interest of the Study

1.5.1. Features of the Films Deposited in the Study

The type of film deposited in this study is hydrocarbon film, a matrix of carbon and hydrogen different from a polymer because there is no associated chain length; the structure is best thought of as a solid solution^{6 – 8, 11, 13, 14}. These materials have a high degree of molecular complexity associated with their matrix, as well as a wide variety of characteristics^{6 – 8, 13}. For example, their microstructure can have varying degrees of crystallinity embedded in an amorphous structure, depending upon the carbon-to-hydrogen ratio,^{6, 10} and the energetics of the absorbed species at the interphase, which is typically controlled by the temperature of the substrate. Moreover, the microstructure can be tuned, energizing the atomic species absorbed onto the surface using the high ion energy density source of the ECR-MW-CVD system.

1.5.2. The Deposition of Hydrocarbon Films

The ECR-MW-CVD system deposited various types of films suitable for making shells for laser fusion experiments. The data from the characterization techniques showed that these films were from 0.2 to 9.8 μm -thick, their refractive indices were from 1.2 to 1.6, their densities were up to 1.8 g/cm^3 , and their hardnesses and stresses were from 0.3 to 12.1 GPa and from 5.2 to 180 GPa. It also showed that these films possessed roughness ranging from 4 to 430 nm-rms over an area of 10,000 μm^2 . However, at pressures < 3 Pa, no deposition was achieved as the plasma conditions favored etching or desorption over deposition or nucleation, and there was no film growth observed at pressures > 7 Pa.

The hydrocarbon films deposited in this study used methane gas as the limiting reactant and hydrogen as dilution gases. Other gas combinations are known to form hydrocarbon films, but this study was limited to these two gases to limit the complexity of the gas- and surface chemistries that occur⁶. All the syntheses were at substrate temperatures $\leq 200^\circ\text{C}$ and pressures between 2.6 – 7.0 Pa. Films were deposited on silicon (1,0,0) and Kapton HN film¹⁶. Depositions were done by changing ECR-MW powers, ECR-MW voltage-to-current ratios or resistances, gas pressures, and methane-to-hydrogen ratios^{9, 10}. Also, by changing the substrate temperature and electrical bias of the substrates^{10–12}.

1.5.3. The Verification-by-Proof Cause-and-Effect Phase

The verification-by-proof cause-and-effect phase was a two-stage process that combined research literature with software. The first step was to arrange the data corresponding to the independent and dependent variables into matrices, graphics, or images. This step employed multiple spreadsheet calculations, basic statistics, image processing, and illustration techniques to record, manage, and analyze the data. The second step was to use these matrices and visual arrangements to verify cause-and-effect between the dependent and independent variables. In this step, the observations were backed up using literature related to the ECR-MW-CVD technique⁹⁻¹², hydrocarbon films^{6,7}, laser fusion experiments¹⁻⁵, and each characterization methodologies used to measure the films' properties.

The study classified the system's processing parameters and the films' properties into three types of variables: independent-variables, dependent-variables, and mixed-variables, where the term mixed-variables refers to those variables that are neither fully independent nor dependent variables. The main independent variables were the substrate temperature, the percentage of methane, the total gas pressure, the processing time, ECR-MW voltage-to-current ratio — or ECR-MW resistance, and the ECR-MW power. Ancillary independent variables were the substrates and the heater temperature. The dependent variables were the thickness, stress, roughness, hardness, density, color, and coating uniformity of the films. The mixed variables were the surface's chemistry and the refractive indices of the films.

1.6. Overview of the Relationship between the ECR-MW-CVD Method, its Ambipolar-State's Character, and the Properties of Vapor Deposited Films

In any vapor deposition method, films are grown according to five phenomena: diffusion, inter-diffusion, desorption, step-nucleation, and 3D-nucleation. Figure 1.6-1 shows the action of these phenomena in the formation of the films¹⁷.

How and which of these phenomena predominate to form a specific type of film is exclusive of each VD method. This statement is true for physical vapor deposition (PVD), where the species inside the plasma are only ionized to bombard a target that ablates and form the film, or for chemical vapor deposition (CVD), where the species inside the gas or plasma react to form ionized radicals, and then, reacted to form the film^{6, 7, 10, 18}.

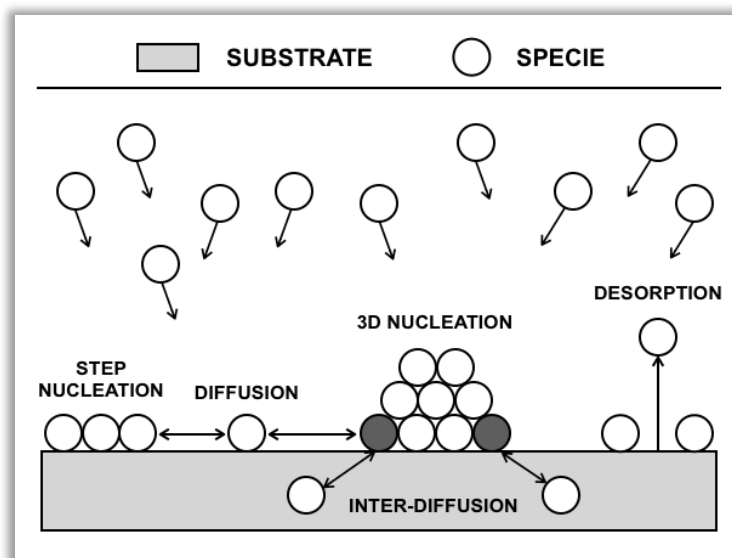


Figure 1.6-1. Atomic transfer phenomena happening in VD methods¹⁷.

In the electron cyclotron – microwave – chemical vapor deposition (ECR-MW-CVD) method, the species inside the plasma are ionized using a moderate electron density and ion energy source. As a result, films can grow at low deposition temperatures due to the moderately high density of energized ions that results from a moderated density of energized electrons inside an ECR-MW plasma^{6, 7, 9–11, 19–21}.

The features of the ECR-MW-CVD method make that method a complementary approach for vapor-deposit films for laser fusion experiments. Currently, these films are deposited on plastic shells via plasma-assisted chemical vapor deposition (PA-CVD) and to helical discharge resonation (HDR). While the ECR-MW-CVD, PA-CVD, and HDR have provided similar electron-plasma confinement, the HDR's source delivers lower ion energy to the species in the plasma than the source of an ECR-MW-CVD's course does. Likewise, the ECR-MW-CVD's source gives lower ion energy to the species in the plasma than the PA-CVD's source does^{2, 9, 10, 17, 20, 21}. The moderate ion bombardment and electron confinement of the ECR-MW-CVD's source makes an ECR-MW-CVD system deposit films with moderate strengths, hardnesses, and densities¹⁷ that are smoother than those films deposited via PA-CVD or HDR^{6, 11, 16–18}.

Nevertheless, the most important thing of the ECR-MW-CVD method is its ambipolar-state's character, which dictates how the plasma species interact at the gas substrate interphase to form a film^{9, 14, 17, 21}. The concept 'ambipolar' refers to the balanced coexistence of the species with opposite characteristics — such as a proton vs. an electron — at the gas substrate interphase. For the specific case of the ECR-MW-CVD method, the ambipolar-state's character of an ECR-MW-CVD system makes the ECR-MW plasma

to be neutrally charged^{22,23}. What is more, the ambipolar-state is transient, in part because of the transient nature of conductivity in the substrate during the deposition process and because of the conditions at which films are deposited. Furthermore, the ECR-MW-CVD method ambipolar-state's character should also be discrete, discriminant, and thus, susceptible to any change in the plasma condition within the ECR-MW-CVD method because of the moderate ion energy and electron density produced by the ECR-MW plasma source.

Ironically, regardless of the ECR-MW-CVD method ambipolar-state's character exists, and it must be depicted no one has ever validated its existence experimentally. The ambipolar-state's character of the ECR-MW-CVD method makes films grow as they do inside an ECR-MW system. Furthermore, research literature shows that the transient, discrete, discriminant, and susceptible of the ambipolar-state's character of the ECR-MW-CVD method can be influenced by intrinsic and extrinsic conditions in the ECR-MW environment. That justifies why the deposition parameters of the ECR-MW-CVD system can be manipulated to control the properties of films while these are deposited.

1.7. The Rest of this Manuscript

The rest of this manuscript shows in more detail the role of the ambipolar-state's character of the ECR-MW-CVD method and its influence on the properties of vapor-deposited films deposited at low energy and near-ambient substrate temperatures. It provides empirical knowledge for making films with a broader range of properties from the perspective of the ambipolar-state's character of the ECR-MW-CVD method.

In addition to that, the rest of this manuscript offers supporting evidence that qualifies the ECR-MW-CVD method as part of the GDP processes to make capsules for laser fusion experiments. In short, it shows that the ECR-MW-CVD method can deposit films with moderate-high densities and modulus at near-ambient substrate temperatures in a controllable way like no other VD method did¹⁻⁵.

1.8. References

01. Gresh LH. Inertial Confinement Fusion: An Introduction—The ENERGY of the STARS. Rochester (NY), United States of America: The University of Rochester; 2009.
02. National Research Council. Assessment of Inertial Confinement Fusion Targets. Washington (DC), United States of America: The National Academies Press; 2013.
03. Lindl JD. Inertial Confinement Fusion: The Quest for Ignition and Energy Gain Using Indirect Drive. Melville (NY), United States of America: American Institute of Physics; 1998.
04. Betti R, Hurricane OA. Inertial-confinement fusion with lasers. *Nature Physics*. 2016;12(1):435–448.
05. Liu CS, Tripathi VK, Eliason B. High-Power Laser-Plasma Interaction. New York (NY), United States of America: Cambridge University Press; 2019.
06. Mort J, Jansen F. Plasma Deposited Thin Films. Boca Raton (FL), United States of America: CRC Press; 1986.
07. Robertson J. Properties of diamond-like carbon. *Journal of Surface and Coatings Technology*. 1992;50(1):185–203.

08. Forgerini FL, Marchiori R. A brief review of mathematical models for thin film growth and surfaces: A possible route to avoid defects in stents. *Biomatter*. 2014;4(1):e28871-1–e28871-11.
09. Geller R. *Electron Cyclotron Resonance Ion Sources and ECR Plasmas*. 1st Ed. Philadelphia (PA), United States of America: IOP Publishing Ltd.; 1996.
10. Lieberman MA, Lichtenberg AJ. *PRINCIPLES OF PLASMA DISCHARGES AND MATERIALS PROCESSING*. New York (NY), United States of America: John Wiley & Sons, Inc.; 1994.
11. Holman JP. *Heat Transfer*. 9th Ed. New York (NY), United States of America: McGraw Hill Publishing Company Limited; 2004.
12. Wilcox EA. *Electric Heating*. St. Haymarket (London), United Kingdom: Technical Publishing Company; 1916.
13. Pouch JJ, Alteravitz SA. *Properties and Characterization of Amorphous Carbon Films*. Brookfield (VT), United States of America: Trans Tech Publications Ltd; 1990.
14. Liu P, Zhang YW, Lu C. Coarsening kinetics of heteroepitaxial islands in nucleationless Stranski-Krastanov growth. *Physical Review B*. 2003;68(1):035402-1–035402-8.
15. Hiemenz PC, Rajagopalan R. *Principles of Colloid and Surface Chemistry*. 3rd Ed. New York (NY), United States of America: Taylor & Francis Group, CRC Press; 1997.
16. DuPont™ Kapton® HN. Wilmington (DE), United States of America: Dupont™; c2019 [accessed 2021 May 18]. <https://www.dupont.com/content/dam/dupont/amer/us/en/products/ei-transformation/documents/DEC-Kapton-HN-datasheet.pdf>.
17. Rossi F. *FUNDAMENTALS IN ION ASSISTED DEPOSITION OF THIN FILMS*. European Commission, Joint Research Centre. Petten, The Netherlands: Research Gate. 1996, January 01. [accessed 2021 May 17]. <https://www.researchgate.net/pu->

blication/295079400_FUNDAMENTALS_IN_ION_ASSISTED_DEPOSITION_OF-
_THIN_FILMS.

18. Williams PF. Plasma Processing of Semiconductors. New York (NY), United States of America: Springer Science & Business Media; 2013.

19. Musil J, Žaček F. Penetration of a strong electromagnetic wave in an inhomogeneous plasma generated by ECR using a magnetic beach. Plasma Physics. 1971;13(6):471–476.

20. AX4555 ECR PLASMA SOURCE: INSTALLATION AND OPERATIONS MANUAL Part No. OM00011 Rev C. Woburn (MA), United States of America: AsTeX Applied Science and Technology, Inc.; 2001.

21. Yasuda H. Plasma Polymerization. Orlando (FL), United States of America: Academic Press Inc.; 1985.

22. Chapman B. Glow Discharge Processes: SPUTTERING AND PLASMA ETCHING. Toronto (ON), Canada: John Wiley & Sons; 1980.

23. Bard AJ, Faulkner LR. Electrochemical Methods: Fundamentals and Applications. 2nd Ed. New York (NY), United States of America: John Wiley & Sons, Inc; 2001.